Correspondence to:
S. L. Danielson,
sldanielson@alaska.edu

Demonstrating a High-Resolution Gulf of Alaska Ocean Circulation Model Forced Across the Coastal Interface by High-Resolution Terrestrial Hydrological Models

Seth L. Danielson[1] , **David F. Hill[2]**, **Katherine S. Hedstrom[1]**, **Jordan Beamer[3]** , and **Enrique Curchitser[4]**

[1]College of Fisheries and Ocean Sciences, University of Alaska Fairbanks, Fairbanks, AK, USA, [2]Civil and Construction Engineering, Oregon State University, Corvallis, OR, USA, [3]Oregon Water Resources Department, Salem, OR, USA, [4]Department of Environmental Sciences, Rutgers University, New Brunswick, NJ, USA

Abstract We demonstrate a linking of moderately high resolution (1 km) terrestrial hydrological models to a 3-D ocean circulation model having similar resolution in the northern Gulf of Alaska, where a distributed line source of freshwater runoff exerts strong influence over the shelf's hydrographic structure and flow dynamics. The model interfacing is accomplished via mass flux boundary conditions through the ocean model coastal wall at all land-ocean adjoining grid cells. Despite the high runoff volume and lack of a coastal mixing estuary, the implementation maintains numerical stability by prescribing depth invariant and surface-intensified inflows at fast and slow discharge grid cells, respectively. Based on comparisons against in situ hydrographic data, the coastal sidewall mass flux boundary condition results in more realistic hindcast surface salinity and salinity gradient fields than models that distribute coastal runoff in the form of spatially distributed precipitation. Correlations with observed thermal and haline monthly anomalies reveal statistically significant hindcast temporal variability during the freshet season when the signal-to-noise ratio is large. Comparisons of ocean models forced by high- and low-resolution hydrological models reveal differences in salinity, surface elevation, and velocity fields, highlighting the value and importance of accurate coastal runoff fields. The model results improve our understanding of the regional influence of runoff on sea level elevations and the distribution and fate of fresh water. Our approach has potential applications to biogeochemical modeling in regions where distributed line source freshwater coastal discharges deliver heat, momentum, and chemical constituents that may influence the marine carbon pump.

Plain Language Summary Fresh precipitation and snow melt runoff from the land enters the salty waters of the Gulf of Alaska, where it plays important roles in determining oceanic temperature and salinity distributions. Salinity distributions influence marine biological productivity, including that of economically important fisheries. Earth system hindcast models help us understand past conditions at times and locations that lack field observations. Models have struggled with generating accurate reproductions of the salinity field in the coastal Gulf of Alaska in part because coastal runoff directly enters relatively deep shelf waters (where mixing is relatively weak) and in part because of insufficiently accurate representations of coastal runoff. In this study we document an improved hindcast, whose results rely on both more accurate depictions of the runoff and the manner of incorporating this runoff into the ocean model. Our approach is compared to model results using more common configurations. This study improves our understanding of the fate of coastal runoff in the northern Gulf of Alaska.

1. Introduction

The Gulf of Alaska (GOA; Figure 1) receives strongly seasonally varying cycles of winds (Wilson & Overland, 1986), coastal freshwater discharge (Beamer et al., 2016; Hill et al., 2015; Neal et al., 2010; Royer, 1982), and incident solar radiation (Dissing & Wendler, 1998) that together support economically important fisheries (Fissel et al., 2017) and define the fate of ocean-advected contaminants, nutrients, plankton, and fresh water (Galt et al., 1991; Stabeno et al., 2016). Of wind, discharge and radiation, the freshwater forcing of regional ocean circulation hindcast models is often the most difficult component to accurately represent in the GOA because this region lacks an intermediate mixing estuary between the land and the
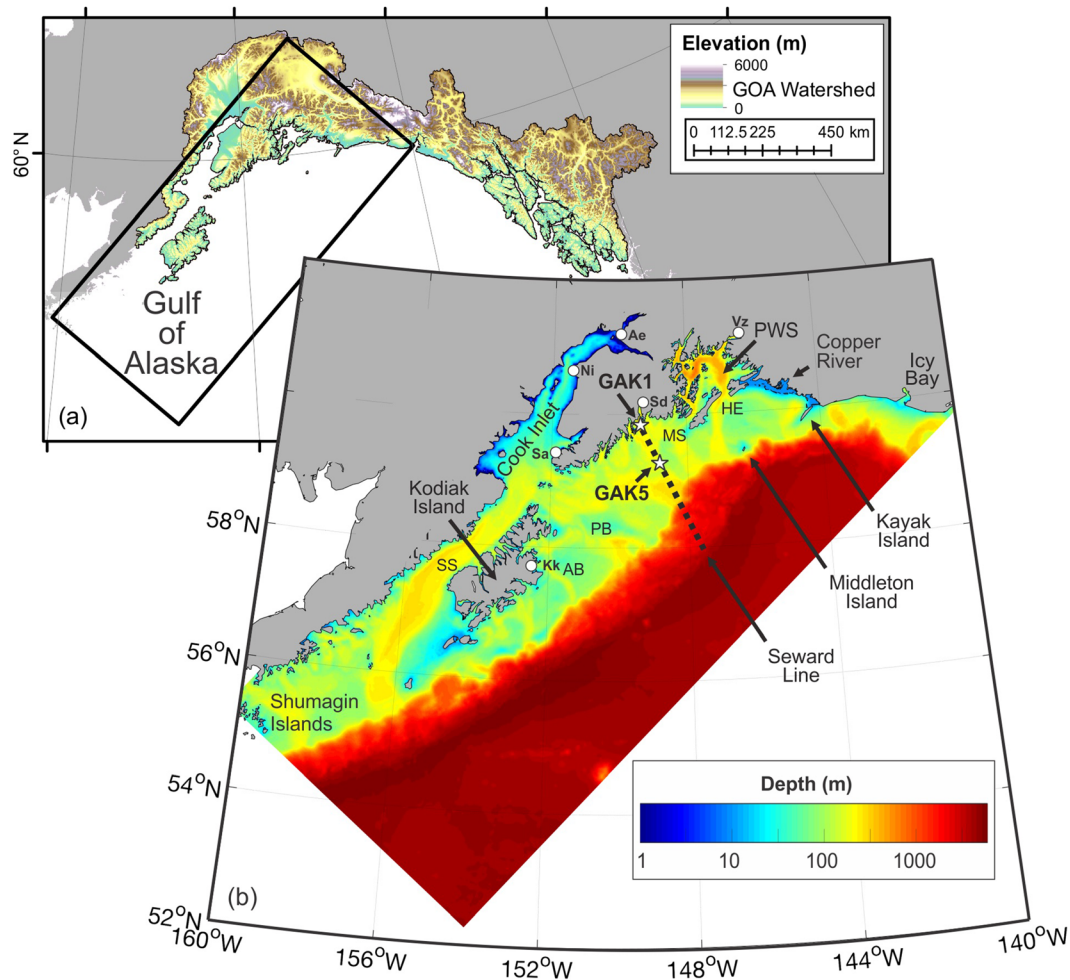
Figure 1. The northern Gulf of Alaska (GOA). Map (a) shows the Beamer et al. (2016) hydrological model domain extent, colored by topographic elevations. The thick black line shows the extent of the NWGOA model. Map (b) shows the NWGOA ocean model bathymetric depths and locations of oceanographic Stations GAK1 and GAK5 (white stars), the Seward Line hydrographic sampling line (black dotted line), place names, and bathymetric features. Abbreviations include AB = Albatross Bank; PB = Portlock Bank; HE = Hinchinbrook Entrance; MS = Montague Strait; SS = Shelikof Strait; PWS = Prince William Sound. Tide gauge stations for Anchorage (Ae), Nikiski (Ni), Seldovia (Sa), Kodiak (Kk), Seward (Sd), and Valdez (Vz) are marked with white circles.

open ocean. This study describes a new approach to implementing coastal freshwater forcing of GOA ocean circulation models in an attempt to improve hindcast modeling, to gain a better understanding of freshwater pathways, and to eventually improve our understanding of the role of fresh water in mediating important biogeochemical cycling processes.

Terrestrial freshwater delivery to the GOA shelf is massive (~800 km^3 yr^{-1}; specific runoff of ~1.8 m) (Beamer et al., 2016; Hill et al., 2015), exerting a dominant influence on the regional physical and biological systems because salinity variations dominate variations in both lateral and vertical density gradients in this region (Carmack, 2007; Royer, 1982). Salinity also controls the variable dynamic topography, including that of the seasonally adjusting Alaska Coastal Current (ACC) (Johnson et al., 1988; Royer, 1979; Stabeno et al., 2016; Weingartner et al., 2005). Variations in salinity play a pivotal role in establishing the depth of winter mixing, which can subsequently impact the renewal of near-surface nutrient concentrations (Janout et al., 2010). Salinity stratification likely helps regulate the timing and magnitude of the GOA spring bloom (Henson, 2007; Strom et al., 2016; Weingartner et al., 2002). Over longer time scales, warming climate is driving year-over-year melting of Alaskan glaciers, providing an additional 50–60 km^3 yr^{-1} of fresh water (Hill et al., 2015; Jacob et al., 2012) to the GOA, and contributing to long-term observed declines in near-surface salinity (Freeland et al., 1997; Kelley, 2015; Royer & Grosch, 2006).

Despite the importance of the coastal discharge, our understanding of its role in regulating oceanic transport pathways, the ecosystem, and the climate system has previously been limited by sparse observations and numerical modeling efforts that have not managed to adequately resolve the marine freshwater system in either space or time. For example, 75% of the GOA runoff comes from small, ungauged coastal rivers that drain the complex mountain topography between the larger gauged interior rivers (Neal et al., 2010; Royer, 1982). While hydrological modeling can fill gaps in the observational record, low- and moderate-resolution global runoff products (e.g., Dai & Trenberth, 2002; Ek et al., 2003; Fekete et al., 2002) do not capture complex processes within small watersheds at the coastal margin or even the bulk coastal discharge magnitude. For example, Fekete et al. (2002) compute runoff on a monthly 0.5° spatial grid, the Dai and Trenberth (2002) data set provides monthly means on a 1° grid; Ek et al. (2003) computations are provided on a 0.25° grid but computed at ~12-km resolution. The Royer (1982) model estimates monthly runoff from the GOA watershed as a whole using precipitation and temperature observations but with very coarse spatial resolution (two aggregated results; one for southeast Alaska and one for south central) that are combined, using time lags applied to the fresh water originating in SE Alaska, to represent the likely freshwater delivery to the northern GOA. The work of J. Wang et al. (2004) applies a moderate-resolution (~4–5 km) spatially explicit modeling approach and a temperature-index model for snow and ice processes but is primarily calibrated to large drainages that are not located close to the coastal zone, thereby discounting large volumes of runoff deriving from the coastal mountainsides. Hill et al. (2015) take statistical approaches that are constrained by gauged streamflow measurements to predict monthly flows at the catchment level. The Beamer et al. (2016) work (1-km spatial grid; daily time step) is the first to use energy-balance methods to model regional snow and ice hydrological processes across the GOA watershed. They calibrate their models with streamflow and glacier mass balance data from coastal mountain watersheds instead of the large interior rivers used by J. Wang et al. (2004).

Previous ocean circulation modeling efforts implement a variety of approaches to handling massive freshwater line source coastal discharge boundary conditions and the associated problem of runaway stratification in ocean models, which can be controlled by constraining the Brunt-Vaisala stratification parameter to some upper limit value (Simpson et al., 1991). Runaway stratification is especially problematic in regions of freshwater influence that lack a mixing estuary (such as the GOA) for a gradual salinity adjustment between the open ocean and the coast. In an idealized modeling setup, Williams et al. (2007) forced a GOA freshwater line source through the coastal sidewall, maintaining stability by using a slightly brackish density anomaly of 1–4 kg m^{-3} rather than pure freshwater input. Some Alaska region studies (Coyle et al., 2012; Dobbins et al., 2009; Hermann et al., 2016; Siedlecki et al., 2017) apply a precipitation-like surface buoyancy line source using the spatially coarse monthly discharge time series of Royer (1982) with enhanced forcing near a select few larger rivers and thermohaline adjustments based on coastal observations. Dobbins et al. (2009) tested three different freshwater input forcing methods (brackish water input, surface freshwater input, and fresh water distributed vertically through the coastal sidewall), settling on a brackish input solution that strongly restores coastal salinity profiles to the observed climatology. Danielson et al. (2011) distribute the low-resolution but interannually varying and spatially variable runoff of Dai et al. (2009) as virtual precipitation. Farrara et al. (2013) and Colas et al. (2013) use the same virtual precipitation approach but employ the temperature-index model of Wang et al. (2004) to define temporal (daily) and spatial (~4 km) variability. Wang et al. (2014) take a hybrid approach, prescribing the Copper River (65,000-km^2 watershed area; 14% of GOA watershed total area) as a point volume and momentum source, with a distributed surface buoyancy line source imposed elsewhere. Coyle et al. (2019) apply the high-resolution forcing of Beamer et al. (2016), also via surface forcing as precipitation. Prescribing runoff as precipitation arbitrarily distributes the fresh water across the ocean surface within some decay distance from shore but it avoids complications associated with model adjustments to a freshwater volume input in the absence of a mixing estuary. However, this approach unrealistically alters the ocean salinity without necessarily changing volume, heat content or other tracers.

With favorable comparisons against individual drainage streamflow records, altimetry data of glacier mass loss (Larsen et al., 2015) and Gravity Recovery and Climate Experiment (GRACE) satellite estimates of water storage across the GOA (Arendt et al., 2013), the hydrological modeling of Beamer et al. (2016) provides an opportunity to reconfigure and reassess coastal discharge forcing in GOA circulation models. Here, we have

two primary objectives. The first is to demonstrate a unique configuration of relatively high resolution models linked across both sides of the marine-terrestrial interface in a region strongly influenced by fresh water. The second is to demonstrate how differences in coastal freshwater runoff implementations (among a suite of hydrological and ocean models) variously propagate into nearshore waters and affect GOA sea levels, salinity distributions, shelf currents, and freshwater pathways.

Model configurations are described in section 2, along with the method of introducing terrestrial runoff into the ocean model and the hydrographic data used for model-data comparisons. Model performance is assessed in section 3, including descriptions of the model's tidal and subtidal circulation fields and freshwater pathways, and by comparing hindcast and observed salinity fields. Discussion and a brief summary are in section 4.

2. Methods

2.1. Ocean and Terrestrial Hindcast Models

Following many previous GOA ocean circulation modeling efforts, we employ the terrain-following framework of the Regional Ocean Modeling System (ROMS) (Hedström, 2018; Marchesiello et al., 2001; Shchepetkin & McWilliams, 2005) as initially set up in the North East Pacific (NEP) (Curchitser et al., 2005). The NEP model is a 10-km horizontal resolution model, and we use integrations from NEP model Version 6 (NEP6) (Danielson et al., 2011) to force a higher-resolution (~1.5 km) domain that extends from Icy Bay to the Shumagin Islands in the GOA (Figure 1b). This higher-resolution grid is termed the North-West GOA (NWGOA) model, and its configuration is a direct code descendant of NEP6. The NWGOA model has 794 grid points in the nominal along-shelf direction (NE to SW) and 362 grid points in the cross-shelf direction, of which more than 2.09×10^5 are ocean grid cells. Boundary and initial conditions for the NEP6 domain are from the global Simple Ocean Data Assimilation (SODA) reanalysis (Carton et al., 2000). In turn, NEP6 provides oceanic boundary conditions to the downscaled and unidirectionally nested NWGOA model (Figure 1b).

We integrate the NWGOA model over 1999–2008, with surface forcing from National Aeronautics and Space Administration (NASA)'s Modern Era Retrospective Analysis for Research and Applications (MERRA) (Rienecker et al., 2011) high-resolution global reanalysis. The MERRA fields provide winds, air temperature, specific humidity, and shortwave and downwelling longwave radiation, subsampled to 3-hourly time steps on a $(1/2)°$ latitude by $(2/3)°$ longitude grid. Air-sea fluxes are computed using bulk formulae (Large & Yeager, 2009) appropriate for high-latitude oceans. Oceanic mixing is computed using a generic length-scale mixing scheme (Umlauf & Burchard, 2003; Warner et al., 2005). Tidal forcing comes from the Oregon State University version TPXO 7.2 tidal inversion based on satellite altimeter sea surface height (SSH) measurements (Egbert & Erofeeva, 2002). A wetting-and-drying algorithm (Warner et al., 2013) is employed to improve the model's performance in shallow and tidally energetic regions such as Cook Inlet and near the Copper River.

Coastal freshwater discharges forcing the NWGOA model are from the coupled land hydrology models described by Beamer et al. (2016). This modeling suite includes MicroMet (Liston & Elder, 2006a), which distributes meteorological variables (station or reanalysis grid points) to the model grid; SnowModel (Liston & Elder, 2006b), an energy-balance snow evolution model, suitable for application both on and off ice surfaces; SoilBal (Beamer et al., 2016), which calculates soil water storage, evapotranspiration, and surface and baseflow runoff; and HydroFlow (Liston & Mernild, 2012), which routes runoff across the landscape to designated basin outlets.

The integrations of Beamer et al. (2016) were calibrated and validated using a combination of U.S. Geological Survey (USGS) streamflow and glacier surface mass balance measurements and were additionally validated against GRACE satellite estimates of water storage. They found that model runs with the Climate Forecast System Reanalysis (CFSR) (Saha et al., 2010) and the North American Regional Reanalysis (NARR) (Mesinger et al., 2006), the latter bias-corrected (BC) to PRISM model (Daly et al., 1994) climatologies, both yielded long-term trends that were consistent with GRACE. While CFSR slightly outperformed NARR-BC in terms of calibration metrics, the CFSR-driven model runs were not yet available at the time of the coupled model runs presented herein. The NARR-BC run had a mean annual precipitation of 930 km^3 yr^{-1}, with

approximately a 1:1 rain-snow fraction. Mean annual runoff is estimated at 870 km^3 yr^{-1} and mean annual evapotranspiration/snow sublimation 125 km^3 yr^{-1}. The water balance shows a net annual loss of 48.5 km^3 yr^{-1}.

2.2. Model Coupling

Our solution to incorporating the high-resolution terrestrial discharge as an ocean model forcing field is an implementation of point-source river inputs at every single NWGOA coastal grid cell by conservatively mapping discharges from Beamer et al. (2016) coastal grid cells onto the corresponding NWGOA coastal grid cells. Laterally forcing the fresh inflow as a daily mean mass flux through the coastal wall at all depth levels allows us to fully specify inflowing momentum, heat, salt, and passive tracer fields, thereby overcoming some of the limitations associated with the virtual precipitation freshwater sources described above. By allowing fresh water to enter the oceanic domain at every coastal grid cell (mainland Alaska and islands), this coupling provides an effective "line source" of fresh water that varies spatially as a function of the catchment basin size and varies temporally as a function of precipitation rates, snow melt rates, and the other factors that influence discharge streamflow.

Testing showed that our model setup, which relies on the Beamer et al. (2016) high-resolution discharge product along with a combination of two input velocity profile types (Figure 2), was able to largely keep the runaway stratification problem under control. The vast majority of coastal points have low discharge rates, and here the inflow was prescribed with a velocity profile that linearly decreased from the surface to the seafloor. At major rivers the inflow was prescribed with a depth-invariant velocity profile in order to promote stronger cross-frontal mixing with the ambient shelf waters. Numerical instability stemming from extremely high inflow rates required an artificial deepening of the local model bottom depth in some locations.

2.3. Data for Model Evaluation

In section 3 we compare temporal fluctuations of modeled hydrography to in situ data collected at Oceanographic Station GAK1, which is located at 59.85°N, 149.47°W in 268 m of water (see Figure 1b). Water column conductivity-temperature-depth (CTD) profiles have been collected regularly at GAK1 since December 1970 (https://doi.org/10.24431/rw1k1b), with casts extending from the surface to within 10 m of the seafloor. Additionally, a mooring with CTD data loggers has been deployed close to the CTD station nearly continuously since 2000 (https://doi.org/10.24431/rw1k18), with sensors at 20- or 30-m depth and each of 60-, 100-, 150-, 200-, and 250-m depths. A composite CTD time series at standard depths is formed by combining the moored and profile data, from which monthly mean values are computed. Monthly anomalies for both the model and the observations are thence formed by subtracting the corresponding monthly mean temperature, salinity, and density from each record's depth-specific monthly mean.

GAK1 is the innermost station of the Seward Line hydrographic transect (Weingartner et al., 2002), which extends over 200 km offshore, to the base of the continental slope (see Figure 1). Following the spring and summer months of snow pack melt and high discharge, September is a month of elevated freshwater content on the Seward Line, with a strongly pronounced ACC front that separates saline midshelf waters from the low-salinity coastal realm. We use September 2007 Seward Line CTD data in the upper 50 m of the water column to illustrate the cross-shelf salinity structure found at this time of year and we use CTD data from Seward Line Station GAK5, which is located 74 km offshore from GAK1 over the northern GOA midshelf region (Figure 1).

To form a surface layer climatology of the late summer and early fall salinity field, we gridded and interpolated CTD data extracted from the World Ocean Database (Boyer et al., 2013). Particularly in the NE GOA in the vicinity of the outflow plume of the Copper River, available data are spatially sparse so observations between August and October were included in this seasonal climatology.

A set of 79 coastal CTD transects that comprise seven repeat sections were conducted in Lower Cook Inlet between 2004 and 2006 (Okkonen et al., 2009). In total, these include 1,225 individual CTD profiles and 99,517 discrete 1-m depth bin observations. We use these data to assess the model's ability to capture inner shelf thermohaline variability downstream from Station GAK1.

For assessing the NWGOA advective field, observationally derived tidal current harmonics parameters are taken from existing compilations (Danielson et al., 2012) and computed directly from raw data obtained
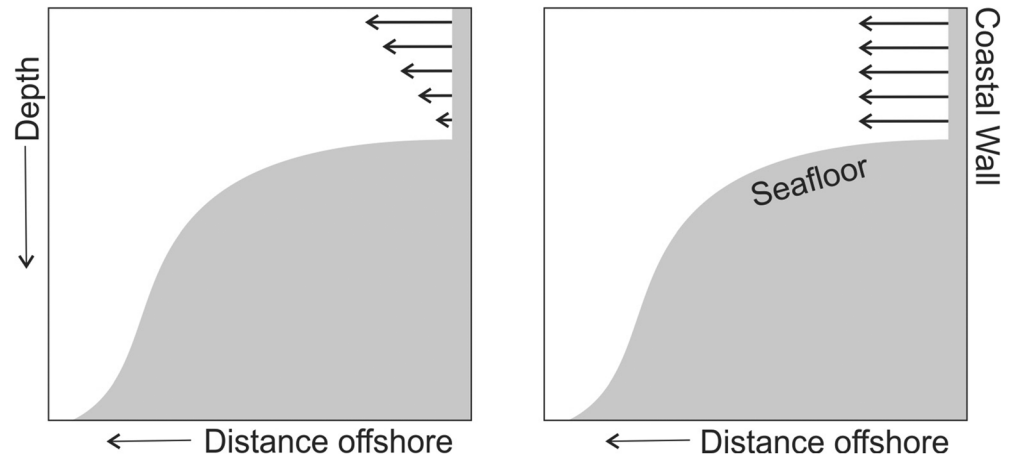
Figure 2. Schematic representing the two velocity inflow profiles used to implement the line source terrestrial discharge forcing of the NWGOA ocean model. Low-volume (left) and high-volume (right) runoff carries volume, momentum, heat, fresh water, and passive tracer fluxes into the ocean through the coastal wall.

at the National Oceanic and Atmospheric Administration's (NOAA's) Currents Measurements Interface for the Study of Tides (CMIST, https://cmist.noaa.gov/cmist/). The CMIST Internet portal provides an archive of data collected by the Center for Operational Oceanographic Products and Services, a branch of NOAA's National Ocean Service. CMIST data sets are typically comprised of 1- to 2-month deployment durations and 6-min averaging ensembles using Teledyne RDI 300-kHz Workhorse acoustic Doppler current profilers (ADCPs). One month of data is sufficient for computation of 29 tidal frequencies, and the tidal current analyses capture the majority of the tidal energy, but the data are insufficient for examination of seasonal changes in the tides due to, for example, the seasonally evolving stratification field.

3. Results

Below, we examine performance of the coupled ocean and terrestrial hydrological models by comparing the NWGOA hindcast hydrographic fields to in situ data and to results of differently configured model integrations. We direct particular focus to showing the impact of freshwater forcing upon salinity distributions, salinity temporal variations, and the fidelity of the model in reproducing available observations (section 3.1). Coastal tide gauge data and moored ADCP data are used to assess the model's tidal elevation and circulation field. The subtidal flow field is quantitatively compared to moored data and qualitatively compared to prior descriptions based on previously summarized sparse collections of current meter mooring and satellite-tracked drifter data sets (section 3.2). Seasonal variability in freshwater pathways as suggested by the model are described and discussed (section 3.3).

3.1. Importance of Fresh Water

Figure 3 shows the monthly climatology of discharge into the GOA from Royer (1982), Beamer et al. (2016), Dai et al. (2009), Ek et al. (2003), and Fekete et al. (2002), the latter three being coarse-to-medium-resolution global products, and the Royer (1982) discharge being a regional estimate based on coarsely aggregated divisional meteorological data. Beamer et al. (2016) find a mean annual discharge into the GOA that is nearly twice that of the global products. This is due to these global products being sufficiently coarse that they do not capture snow and ice processes well in complex, highly variable terrain. It is also due to some global products simply masking out glacier areas and ignoring the hydrology there
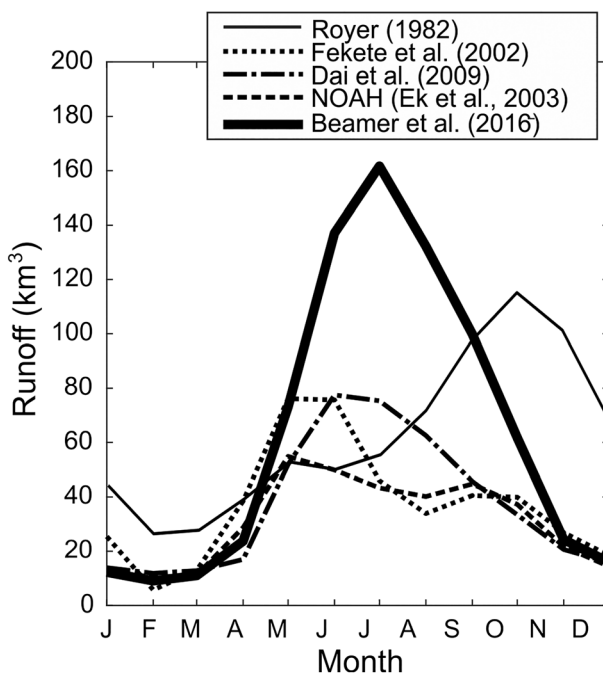

Figure 3. Mean seasonal hydrographs of estimated coastal discharge into the Gulf of Alaska from five different runoff products that prescribe discharge with differing amplitudes and seasonal timing.
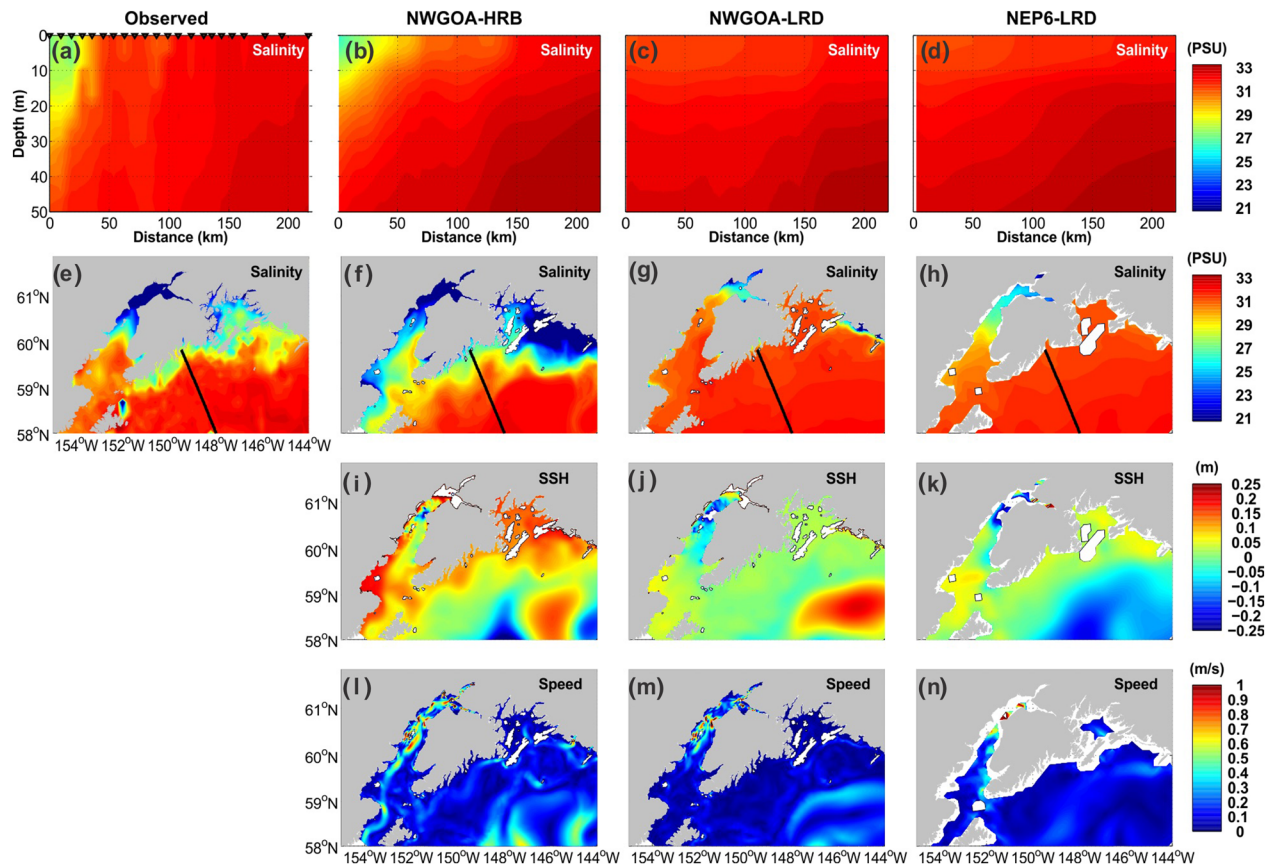
Figure 4. Comparison of observations and three different model integrations. All panels with model results show averages for the month of September 2007. In situ CTD data (left-hand column) along with the NWGOA-HRB model forced with the Beamer et al. (2016) discharge (second column), the NWGOA-LRD model forced with the Dai et al. (2009) discharge (third column), and the NEP6-LRD model forced with the Dai et al. (2009) discharge (right column). The top row (a–d) shows Seward Line cross sections of salinity from the models and CTD data collected over 8–10 September 2007. CTD casts were made at the inverted triangle marks shown on the upper left panel, and the coast is on the left side of each cross section. The black line in the second row shows the location of the cross-section transects that are depicted in the top row. The second row panels (e–h) show surface salinities with the leftmost panel using August–October data from the World Ocean Database (Boyer et al., 2013). The third row panels (i–k) show modeled sea surface elevation and fourth row panels (l–n) show the modeled magnitude of surface currents.

altogether. The Royer (1982) runoff model has an annual magnitude comparable to the Beamer et al. (2016) model. However, the seasonal variation is dramatically different, with a strong rain-driven peak in the autumn. Additionally, and as previously noted, the Royer (1982) model is not spatially explicit. It provides a single runoff value for southeast Alaska, and a second runoff value for south central Alaska. The comparison (Figure 3) demonstrates the importance of applying domain-specific knowledge and of resolving relevant processes when configuring hydrological models. Naturally, errors in discharge forcing functions have downstream consequences in ocean modeling applications.

For evaluation of various model configurations, the leftmost column of Figure 4 shows CTD data depicting a representative Seward Line salinity cross section (Figure 4a) and a plan view climatology (Figure 4e) of the surface salinity from late summer and early fall. Columns two and three of Figure 4 show the NWGOA model forced with the high-resolution Beamer et al. (2016) (hereafter, HRB) and the low-resolution Dai et al. (2009) (hereafter, LRD) discharges, respectively. Column four of Figure 4 shows NEP6 model results forced with the LRD runoff. The NWGOA-HRB integration was driven by a lateral mass flux through the coastal sidewall as described in section 2; following common practice, the NWGOA-LRD and NEP6-LRD runs were forced with the surface freshwater flux imposed as a virtual precipitation. The fresh water was deposited uniformly across the five grid cells closest to shore, resulting in a cross-shelf distribution length scale of about 8 km for the NWGOA-LRD model and 50 km for the NEP6-LRD model.
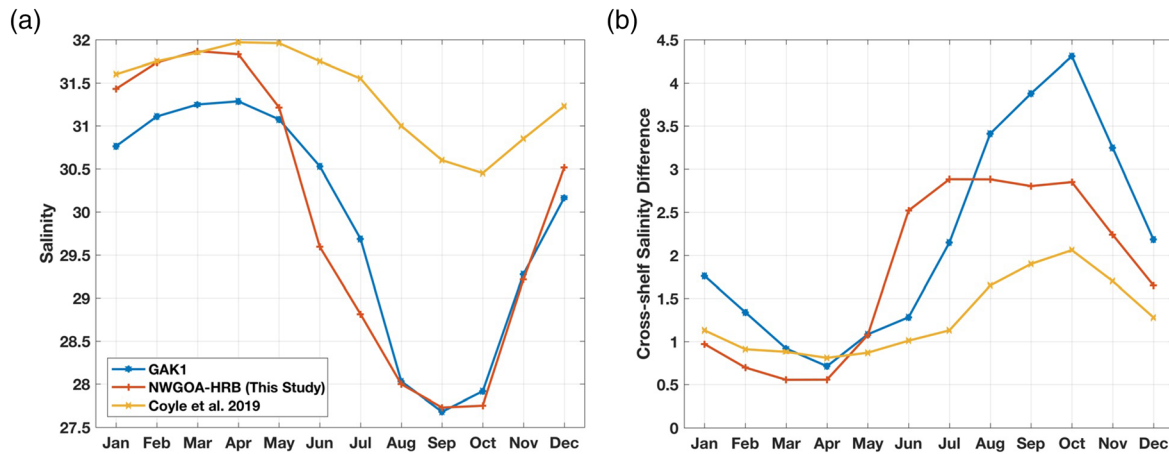
Figure 5. (a) Monthly climatology of the near surface (0- to 25-m average) salinity from Oceanographic Station GAK1 (*) CTD data along with the monthly climatology over the same depth range from two different model integrations. Both models use the high-resolution Beamer et al. (2016) HRB discharge as a freshwater boundary condition. The NWGOA-HRB (+) results apply the coastal discharge as a mass flux through the sidewall. The Coyle et al. (2019) (x) results apply the coastal discharge as distributed precipitation. (b) Cross-shelf salinity difference computed as the upper 25-m salinity at GAK5 minus that at GAK1 as resolved by observations (*), the NWGOA-HRB model (+) and the Coyle et al. (2019) model (x). There are no GAK5 data in January and February (missing data replaced by interpolation); November has only one GAK1 occupation.

The NWGOA-HRB model (Figure 4b/4f) comes closest to reproducing the observed (Figure 4a/4e) dynamic range and spatial distributions that characterize the in situ CTD salinity data. Ship data are sparse between Middleton Island and the Copper River (Figure 4e) in the historic data archives but clearly the NWGOA-HRB (Figure 4f) model results are somewhat fresher than the surface observations in this region. Small wiggles shown in the CTD-based plan view (Figure 4e) are not due to frontal meanders or instabilities but rather the paucity of data. Note that the NARR-BC total runoff (870 km^3) is appreciably greater than the CFSR runoff (760 km^3), which Beamer et al. (2016) objectively found to provide the "best" discharge of the reanalysis products tested. Using CFSR discharge to force the NWGOA model should yield closer agreement between the model results and observations. Comparisons (Figure 4a/4b) also suggest that the NWGOA model stratifies somewhat too strongly close to the surface. The model lacks a wind-wave mixing parameterization, implementation of which could both deepen the surface mixed layer and increase surface salinities.

The HRB forcing and model setup also exerts control over the SSH and velocity fields by redistributing surface anomalies and sharpening frontal zones and their associated velocity jets (rows three and four of Figure 4). We note that the coastal freshwater wedge depicted close to shore west of Prince William Sound (Figure 4b) and the nearshore velocity jets (Figure 4l) here and in western Cook Inlet and Shelikof Strait are clear manifestations of the ACC structure (Stabeno et al., 2016; Weingartner et al., 2005). In contrast, the ACC is only weakly present as a low-salinity coastal wedge of fresh water with only modest velocity signatures in both of the LRD model runs.

Station GAK1 is always situated shoreward of the ACC front but not within the sheltered waters of the adjacent fjord, so data from this location are appropriate for assessing the NWGOA model's response to terrestrial runoff. It is also the most highly sampled oceanographic station in the coastal GOA, with a well-resolved monthly climatology. We use data from GAK1 to assess the ability of the various models to hindcast nearshore salinities.

In Figure 5a we compare the GAK1 climatological monthly near-surface (0 to 25-m average) salinity against the monthly climatology from the NWGOA-HRB model and the monthly climatology of Coyle et al. (2019). As we are interested in well reproducing the mean system state, we compare the monthly climatology of each data set to avoid potential bias from instantaneous snapshots. The Coyle et al. (2019) freshwater forcing is based on the same high-resolution Beamer et al. (2016) coastal discharge that is used in our study, but Coyle et al. (2019) implement the fresh water as a virtual precipitation at the surface with a cross-shelf *e*-folding decay scale of 30 km. The comparison in Figure 5 suggests that the 30-km decay scale deposits

coastal runoff on average too far offshore or it allows too much fresh water to leak offshore, because even though the Coyle et al. (2019) model is based on the HRB discharge volume, the salinity climatology found here is closer to that of the even saltier NWGOA-LRD climatology (not shown in Figure 5) than to that observed at GAK1. The annual mean difference between the GAK1 climatology and the NWGOA-HRB climatology is -0.1 ± 0.3, and the annual mean difference between the GAK1 climatology and the Coyle et al. (2019) results is -1.5 ± 0.5. It is not presently clear why the Coyle et al. (2019) results exhibit a mean freshwater deficit. Relative to the observations, the Coyle et al. (2019) integration is too saline by about 0.5–1 over December through June and too saline by about 2–3 over July through November. The annual spring-to-fall range of the Coyle et al. (2019) model (~1.5) is less than half of the observed range of (~3.5). The NWGOA-HRB model is too saline by about 0.5 over January through April, possibly suggesting that in fall months too much fresh water is fluxed offshore and hinting that the NWGOA-HRB model could benefit from more vigorous fall and winter mixing in the vertical direction.

Royer (1982) and Weingartner et al. (2005) show that because salinity is a proxy for density in the northern GOA, we can use the near surface cross-shelf salinity gradient to estimate along-shelf transport, which affects freshwater transport (FWT) and the advection of larvae and other plankton. The CTD data, the NWGOA-HRB model, and the Coyle et al. (2019) model all show cross-shelf (GAK1 to GAK5) increases of salinity of between 0.5 and 0.8 at the end of winter (Figure 5b). The observations exhibit a salinity gradient seasonal range of about 3.5 from end of winter to early fall, while the NWGOA-HRB and Coyle et al. (2019) integrations show seasonal changes of 2.3 and 1.3, respectively. Simple relations show that density gradients drive both buoyancy-driven steady flows and eddy fluxes (Spall & Chapman, 1998; Weingartner et al., 2005), so Figure 5b suggests that alongshore baroclinic transports and offshore baroclinic eddy fluxes are likely underestimated by approximately a factor of 2 in the July to October Coyle et al. (2019) model integrations. The NWGOA-HRB model sets up a strong cross-shelf frontal system about a month earlier than the observations, and it fails to additionally increase the GAK1-to-GAK5 gradient through the whole summer into October.

Using a similar GOA model ROMS model setup, Dobbins et al. (2009) tested a coastal wall lateral freshwater line source using the Royer (1982) discharge but found that the model did not retain sufficient fresh water in the nearshore region: the May through August average surface salinity had the 26 isohaline outcropping ~100 km offshore near the continental shelf break (their Figure 14d). In contrast, the NWGOA-HRB surface salinity field in September 2007, which follows an entire summer's worth of freshwater accumulation on the shelf, shows the 29 isohaline in the midst of the ACC front, about 40 km offshore on the Seward Line (see Figure 4f). The above comparisons to Dobbins et al. (2009) and to Coyle et al. (2019) suggest that two factors greatly influence the modeled freshwater distributions over the continental shelf: the quality of the coastal runoff forcing function and the manner in which fresh water is introduced into the model.

To show the importance of the manner in which fresh water is introduced to the model, we conduct a series of three NWGOA model integrations, each computed over January to May 2007 (Figure 6). The first integration is run with no coastal freshwater forcing, and the resulting surface salinity is between 32 and 33 nearly everywhere, except in northern Cook Inlet where the residual influence of ice brine formation and/or evaporation leaves a positive salinity anomaly. The second integration applies the HRB Beamer et al. (2016) discharge in the form of precipitation evenly over the inner shelf to 30 km offshore (Figure 6b). In this case the runaway stratification takes hold, and the 26 isohaline is found close to the shelf break (similar to that of the runaway stratification found by Dobbins et al., 2009). The third integration shows the results using the same HRB Beamer et al. (2016) boundary condition but for the case of the sidewall mass flux forcing (Figure 6c).

We turn now to additional comparisons of the NWGOA model relative to shipboard hydrography in order to better understand this model's ability to capture monthly and seasonal hydrographic variations. Subtracting climatological monthly means from the NWGOA-HRB model results and the observations, we create monthly anomalies of temperature, salinity and dynamic height for the 10-year hindcast. We assume that each month provides an independent sample.

Figure 7 shows that the hindcast reproduces GAK1 monthly anomalies of temperature, salinity, and dynamic height with varying levels of fidelity through the water column and through seasons. For salinity
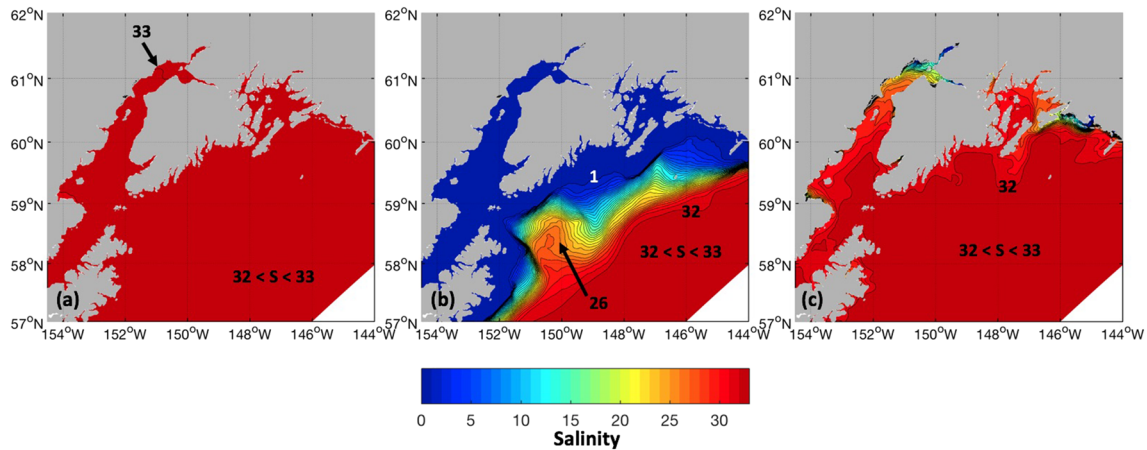
Figure 6. NWGOA model integrations showing the average May 2007 surface salinity for the cases of (a) no coastal freshwater input, (b) the Beamer et al. (2016) fresh water applied as precipitation over the inner shelf, and (c) the Beamer et al. (2016) fresh water applied as a mass flux through the coastal sidewall at every ocean model land grid point. All plots are contoured in steps of 1 from salinity 0 to 33.

(Figure 7b), the strongest correlations ($r = 0.5$–0.6, $p < 0.05$) are found near the surface (10- to 20-m depths) and in the lower portion of the water column (below 200-m depth) in spring (April–June). This season corresponds to the rapid annual increase of coastal discharge caused by the spring snow pack melt and often includes the annual discharge peak in June (Beamer et al., 2016). In summer (July–September), the maximum near-surface salinity correlation weakens ($r \sim 0.4$, $p < 0.05$) and is located slightly deeper in the water column (20–30 m), while the correlation remains near $r = 0.5$ at 200-m depth. The model mostly does not reproduce any statistically significant portion of the observed anomalies in fall and winter (October–March). This time of year is unsurprisingly the most difficult to hindcast, as the runoff rate is low and the signal-to-noise ratio for salinity is small.

The NWGOA-HRB model also exhibits some success in hindcasting temperature and dynamic height fluctuations (Figure 7a/7c). Temperature anomalies are best hindcast ($r \sim 0.9$, $p < 0.001$) in the first half of the year (January–June). Except for late in the year, when fall winds begin to destratify the water column, the maximum temperature correlations occur in the middle of the water column. The modeled 0- to 200-dbar
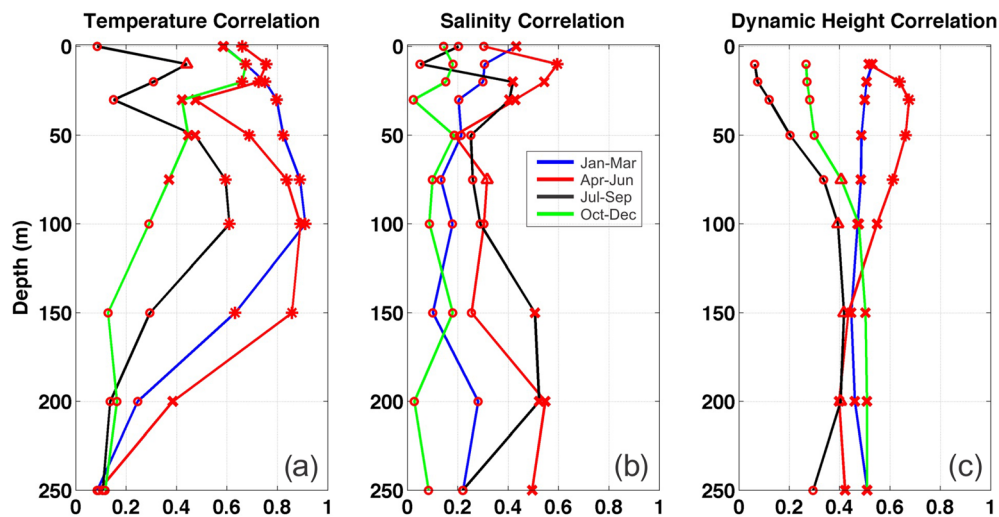

Figure 7. Correlation coefficients (r) between monthly anomalies of observations made at coastal monitoring station GAK1 and monthly anomalies of hindcasts from the NWGOA-HRB Ocean model. Parameters include temperature (a), salinity (b), and dynamic height referenced to the surface (c). Line colors represent January–March (blue), April–June (red), July–September (black), and October–December (green). Symbols show correlations that are not significant (circles) and significant at the 90%, 95%, and 99% levels (triangles, crosses, and asterisks, respectively).

Table 1
Bulk Statistics of the Temperature and Salinity for the Lower Cook Inlet CTDs

Transect	N	T mean (°C)		S mean		T σ (°C)		S σ		Temperature correlation	Salinity correlation
		M	O	M	O	M	O	M	O		
1	18	7.49	7.02	31.75	32.30	1.78	2.04	0.49	0.95	**0.85**	**0.74**
2	14	7.09	6.61	31.71	32.35	2.02	2.14	0.63	1.36	**0.93**	**0.85**
3	16	8.79	7.80	30.35	30.18	2.94	2.79	1.05	2.12	**0.95**	**0.81**
4	17	7.99	7.44	31.19	31.47	2.47	2.73	0.48	0.91	**0.95**	**0.77**
5	8	9.75	7.72	25.24	26.46	3.86	2.39	1.84	2.74	**0.97**	0.38
6	4	8.55	7.72	31.60	32.18	1.33	1.84	0.58	1.28	0.80	0.80
7	4	10.12	9.41	30.86	30.74	0.72	1.58	0.67	1.50	0.50	0.66

Note. Parameters include transect number (1–7), the number of occupations (N), the temperature (T) and salinity (S) mean, T and S standard deviation (σ), and the Pearson's correlation between the modeled (M) and observed (O) data sets. Correlations that are significant for $N - 2$ degrees of freedom at the 95% level for a one-tailed test are shown in bold type.

dynamic height anomaly is significantly correlated with the observed anomaly in all seasons ($p < 0.05$ except $p < 0.1$ for spring) within a fairly narrow range of correlation coefficients of $r = 0.4$–0.5. Weingartner et al. (2005) showed that the GAK1 0- to 200-dbar dynamic height is a proxy for the ACC June–August baroclinic ($r = 0.93$, $p < 0.05$) and FWTs ($r = 0.79$, $p < 0.05$) and also a proxy for the ACC November–May FWT ($r = 0.62$, $p < 0.05$) and freshwater content ($r = 0.85$, $p < 0.05$). Statistically significant prediction of the dynamic height monthly anomalies is a necessary step toward being able to eventually link atmospheric and terrestrial processes that drive discharge fluctuations with their downstream consequences for the marine system.

Comparisons of the model output to CTD data from lower Cook Inlet suggest that the model stratification is somewhat strong on average (overly warm and fresh at the surface and overly cool and salty at depth). The model-observed Pearson's cross correlation is $r = 0.89$ with $p < 0.001$ for temperature and $r = 0.58$ with $p < 0.001$ for salinity. On a transect-by-transect basis, Table 1 shows that the transects with the fewest number of observations (Transects 5, 6, and 7) also have the weakest correlations. In all comparisons that result in significant correlations, the correlation of the temperature fields is stronger than the correlation of the salinity fields. The average temperature offset, with the observations slightly warmer than the model, is 0.65°C ($\sigma = 1.07$) and 58% of the observations were associated with a hindcast value that was within 1°C of the observations; 90% are within 2°C. For salinity, the observations are slightly less saline than the model on average with a mean offset of 0.47 ($\sigma = 1.05$) and 66% of all observations were associated with a hindcast salinity that was within 1 salinity unit of that observed, while 95% are within 2 salinity units. Combined, 43% of the hindcast-observation pairs for the 79 transects simultaneously agree to within 1 (°C and salinity units) for both temperature and salinity. For a threshold of 2 (°C and salinity units), 86% of the hindcast values fall within the range.

3.2. Tides and Currents

The shelf hydrographic structure (Figure 4) reflects the net influence of forcing that modifies oceanic heat and freshwater contents (e.g., runoff and surface heat fluxes) combined with advection and mixing processes. The baroclinic density field, for example, contributes to the shelf circulation in the form of the ACC jet (Royer, 1982; Weingartner et al., 2005). Particularly in the coastal realm, tides provide an important source of mixing energy and the tides and subtidal flows together help determine the structure and location of density fronts and vertical stratification (e.g., Simpson, 1997) as the coastal discharge spreads and adjusts into the marine realm.

Harmonic analysis applied to observed current meter mooring and modeled current velocity time series (Pawlowicz et al., 2002) shows that the model manages to reproduce observed M_2 semidiurnal tidal amplitudes and current ellipses (Figure 8) with appreciable fidelity. The character of the tidal ellipses reveals the strong frictional control that shallow regions and passages of tight constriction impart, with ellipses in these regions being often nearly rectilinear and ellipses in less constricted regions being more circular. Similar ellipse patterns, though of smaller magnitude, are found for the dominant diurnal constituent K_1 (not shown). We note that the model accurately produces ellipse magnitudes in some constricted regions, such
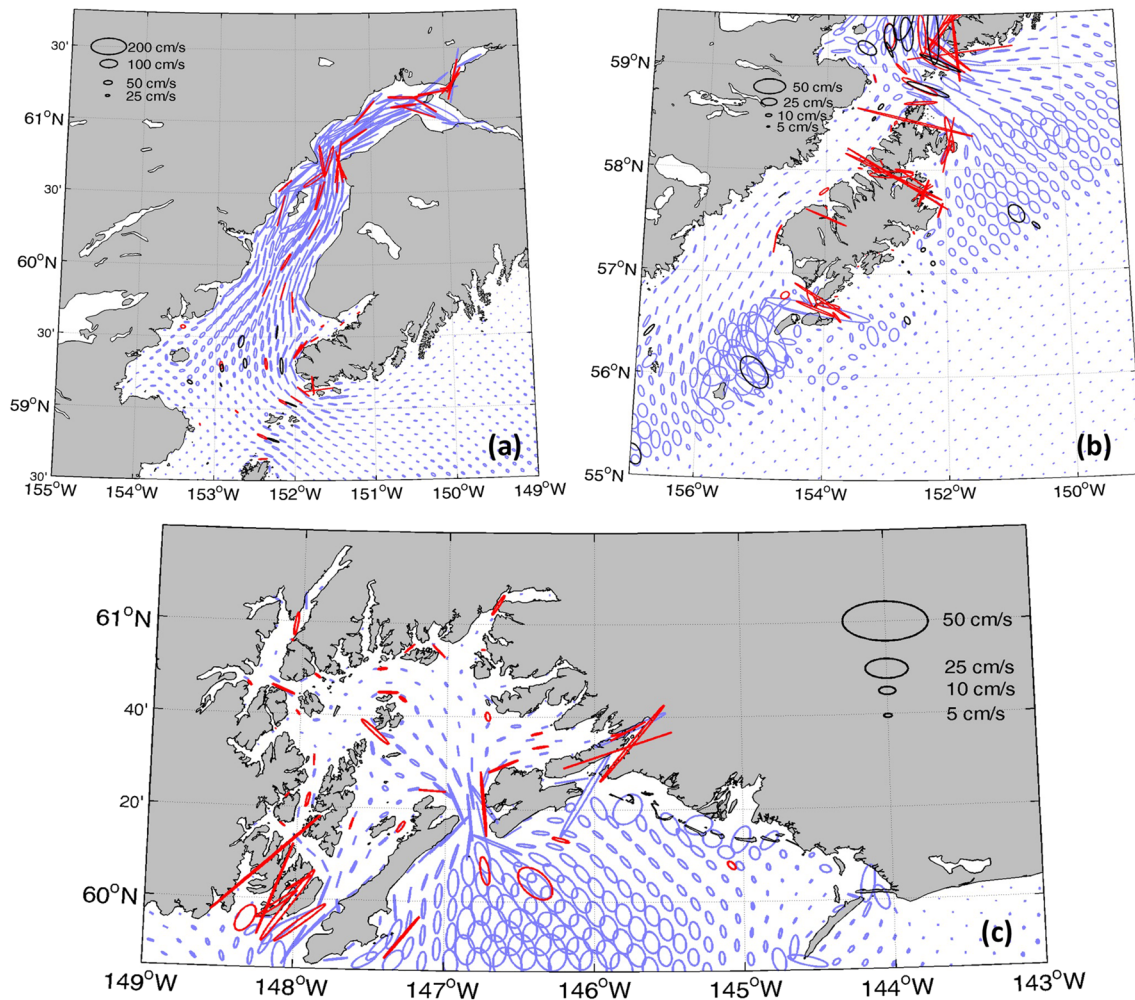
Figure 8. Semidiurnal tidal constituent M_2 tidal ellipses from Cook Inlet (a), near Kodiak Island (b), and Prince William Sound and the Copper River (c) from the model (blue ellipses), and observed based on oceanographic moorings (red ellipses = vertically averaged acoustic Doppler current profiler data; black ellipses = subsurface rotary current meter). Ellipses are shown from every fifth model grid point. Scale ellipses have an eccentricity ratio of 1:2 and the denoted magnitude identifies the semimajor ellipse axis length.

as the passages connecting Prince William Sound to the greater GOA, but also has difficulty in reproducing observed tidal ellipse magnitudes at some sites close to Kodiak Island. Many of these passages are often not well resolved by even the NWGOA model's relatively high horizontal resolution.

The Figure 8 cotidal charts also compare reasonably well to amplitude and phase patterns depicted in prior Cook Inlet and GOA tide model and observation studies (e.g., Foreman et al., 2000; Muench & Schumacher, 1980). A weak but discernable enhancement of the K_1 constituent appears along the outer shelf region. Similar trapping of the diurnal constituent was observed in the modeling by Foreman et al. (2000), whose high-resolution barotropic finite element model was well configured to resolve the shelf break topography although the Foreman et al. (2000) model was a hybrid of the 5-min ETOPO-5 elevation model and an early version of the Smith and Sandwell (1997) satellite gravimetrics bathymetry. Neither of these bathymetric data sets are today considered state of the art. The Foreman et al. (2000) model was two-dimensional, and the authors point out that the structure of the amplitudes and phases are presumably somewhat less accurate with such a setup. Nonetheless, our results depict a K_1 amplitude greatest near the Kodiak Island shelf break and weaker farther along the slope to the east. We find also that K_1 currents are enhanced to the south and east of Kodiak.

For the Anchorage tide gauge station amplitude (Table 2 and Figure 9, upper panel), the minimum root-mean-square difference (RMSD) between the modeled and observed time series is 0.61 m with a Pearson's

Table 2

Comparison of Observed and Modeled Tidal Height Harmonics Parameters (M_2, S_2, K_1, and O_1) for Sea Level Gauges at Stations Located in Anchorage, Kodiak, Nikiski, Seldovia, Seward, and Valdez

Station	Tidal constituent	Amplitude (m)		Phase (°)	
		Model	Observed	Model	Observed
Anchorage	M_2	3.51	3.57	132	103
	S_2	0.76	0.8	160	147
	K_1	0.62	0.89	331	345
	O_1	0.16	0.39	315	334
Kodiak	M_2	0.92	0.97	314	308
	S_2	0.25	0.27	339	343
	K_1	0.44	0.53	303	290
	O_1	0.22	0.25	299	267
Nikiski	M_2	3.04	2.5	61	33
	S_2	0.83	0.69	85	67
	K_1	0.91	0.85	302	311
	O_1	0.43	0.39	298	296
Seldovia	M_2	1.81	2.23	338	325
	S_2	0.53	0.67	0	1
	K_1	0.64	0.76	285	282
	O_1	0.29	0.36	279	262
Seward	M_2	1.15	1.2	301	288
	S_2	0.32	0.34	323	322
	K_1	0.51	0.62	287	275
	O_1	0.25	0.3	281	254
Valdez	M_2	1.31	1.39	300	288
	S_2	0.37	0.4	322	322
	K_1	0.55	0.67	286	274
	O_1	0.28	0.32	280	253

cross correlation of $r = 0.96$ for a time lag of 1 hr (model lagging observations). This lag corresponds nearly exactly to the computed 29° M_2 phase offset between the model and observations (Table 1). In aggregate, with a 1-hr offset, the model reproduces 92% of the observed variance at Anchorage with an error that is typically ~15% of the instantaneous amplitude. For the tide gauge station at Kodiak at the opposite side of Cook Inlet (Figure 9, lower panel), the maximum correlation for the same time interval occurs at zero phase lag with a correlation of $r = 0.96$ and RMSD of 0.21 m. For the six stations shown in Table 2, the model agrees with the observed harmonics amplitudes and phases to within 12 ± 8 cm and $13 \pm 6°$, respectively.

Subtidal flow characteristics were computed for the model and mooring records at the locations of 24 Cook Inlet tide moorings, using the same time interval for each pair. The comparisons suggest that the modeled flow field is somewhat more energetic than the observations, although overlapping error bars show that the aggregated result differences are not statistically significant at the 95% confidence level. For example, the subtidal hindcast net speed from the moorings is 19.8 ± 7.4 cm/s, while the observations show 10.4 ± 3.0 cm/s. We find similarly offset but non-significant differences when we compare flow variances, flow covariances, mean kinetic energies, and eddy kinetic energies. Computation of the principal axis of variation showed that as a ratio relative to the variance of the dominant flow axis, the modeled minor axis of variation is $35 \pm 10\%$, while the observed minor axis is $44 \pm 8\%$. The modeled subtidal flow field showed $86.8 \pm 5.4\%$ of the variance to be aligned with the principal axis of variation (range of 61.3–100%), while the observations showed $83.1 \pm 4.5\%$ (range of 55.4–97.5%). Longer observational records would allow us to better show the differences between the model and actual current fields.

Mean climatological hindcast surface and near-seafloor circulation fields (Figure 10) depict the broad and swift Alaskan Stream flowing along the shelf break (Reed, 1984) and the narrow and swift ACC flowing along the shoreline and aligned with the baroclinic front that develops on the offshore side of the coastal freshwater plume (Royer, 1982). The heavily time-averaged surface flow in Figure 8 exhibits a relatively smooth mean field having long (~100 km) length scales and swiftest currents (>20 cm s^{-1}) that are predominantly directed in the along-shelf (nominally westward) orientation, in reasonable agreement with gridded satellite-tracked drifter observations (Stabeno et al., 2016). Surface flows of all speeds exhibit a strong tendency for bathymetric steering, despite layer decoupling induced by stratification and the relatively deep (150–300 m) bottom depths found over most of the GOA shelf (Figure 1). Satellite-tracked drifters in the GOA even at 40-m depth exhibit the tendency for waters to flow up the eastern side of the canyons then turn and flow down the western side (Ladd et al., 2005). The near-bottom flow field exhibits much weaker mean flow than at the surface and with shorter length scales, but the effect of seafloor topographic steering is still clear. Such pathways represent conduits for nutrient-rich waters and plankton to leave the basin and advect onto the midshelf and inner-shelf domains (Hermann et al., 2009; Mordy et al., 2019). The model depicts surface flow into Prince William Sound through Hinchinbrook Entrance and out of the Sound through Montague Strait, along with bidirectional subsurface flows in both straits (Halverson et al., 2013; Niebauer et al., 1994).

The NWGOA model develops a weak but persistent anticyclonic flow around and in close proximity to Kodiak Island. This flow field is consistent with the cross-strait shear shown in Stabeno et al. (1995) and Stabeno et al. (2016) and the southward flowing branch of the ACC that heads toward the southwest along the southeastern shore of Kodiak. However, we are not aware of reports of northward flowing current on the Kodiak side of Shelikof Strait that extends the length of the island. Such a flow would be consistent with a coastal buoyancy-driven flow forced by island runoff, that of a tidally rectified flow, or of a flow in which nearshore mixing generates persistent cross-shore density gradients.
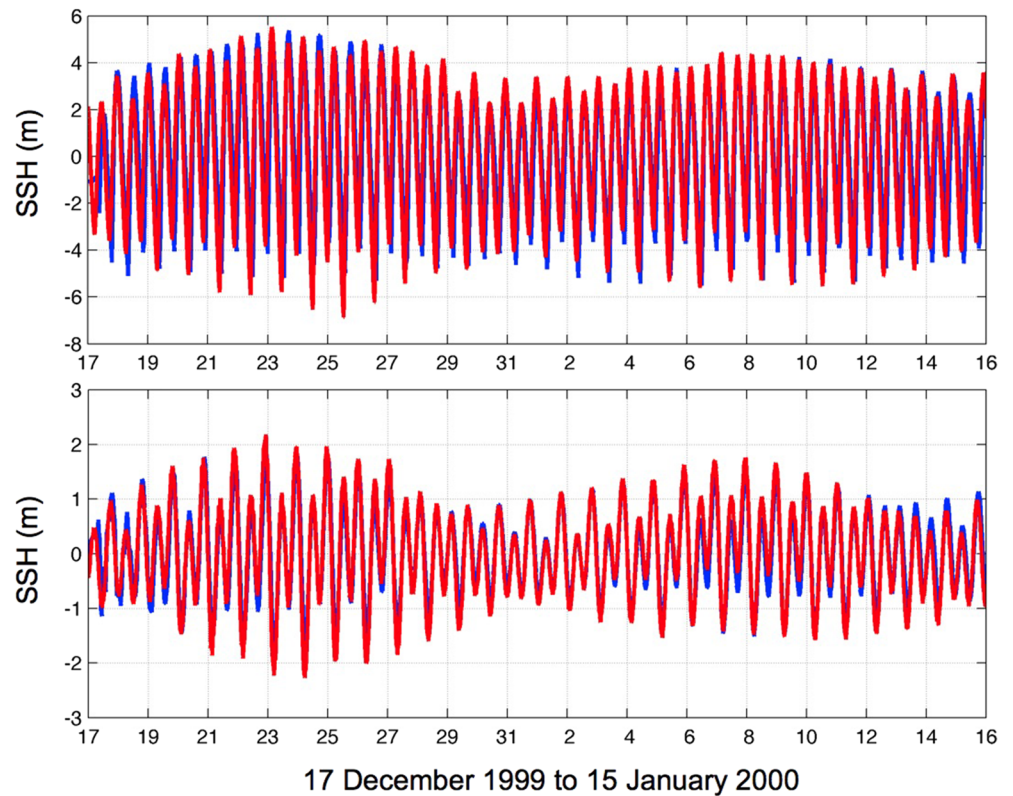
Figure 9. One month of modeled (blue) and observed (red) sea surface height (SSH) at the Anchorage (upper panel) and Kodiak (lower panel) tide stations in December and January 2000.
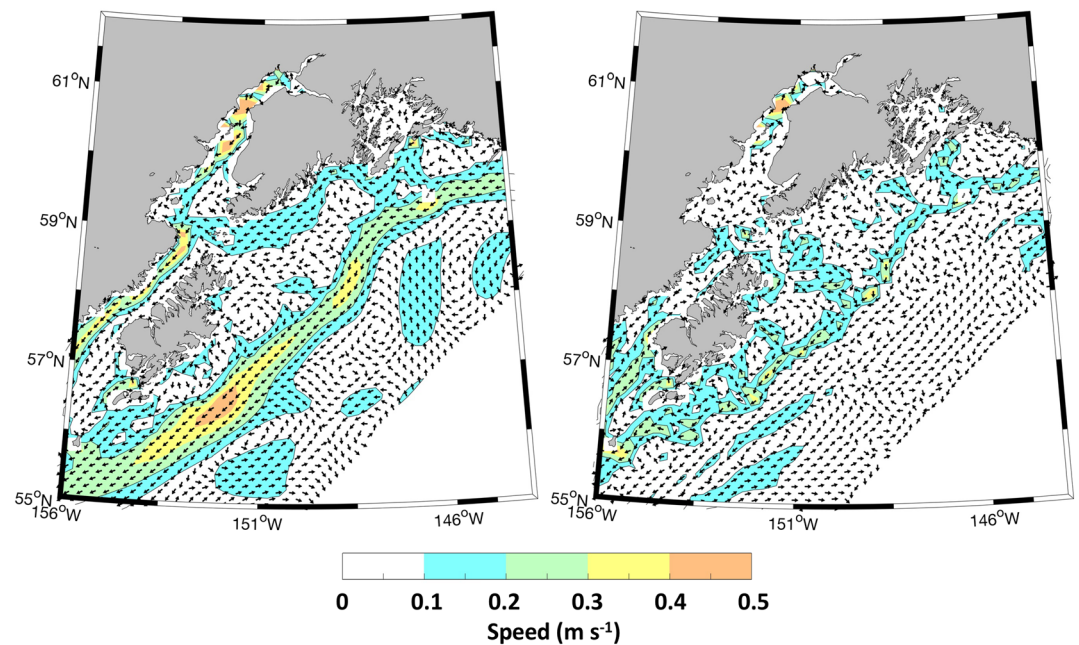

Figure 10. NWGOA modeled surface (left) and near-seafloor (right) subtidal velocity flow fields averaged over the entire 10-year hindcast. Vectors are shown at one out of every 100 model grid points. Arrows denote flow direction and colors denote flow speed in m s^{-1}.
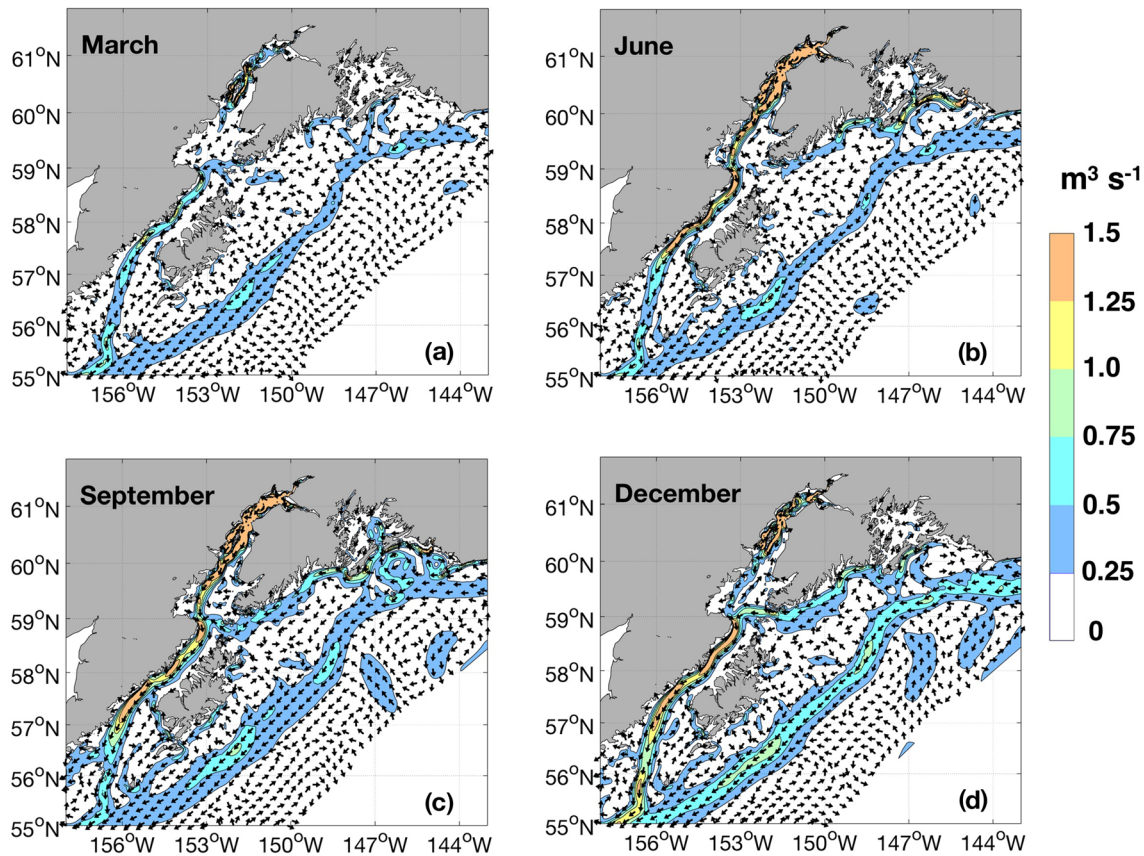
Figure 11. Freshwater transport (m^3 s^{-1}) integrated over the upper 50 m of the water column in March (a), June (b), September (c), and December (d) and averaged over the 1999–2008 NWGOA-HRB model run. Reference salinity is 33.8. Black arrows show the direction of transport and colors show the magnitude.

3.3. Freshwater Pathways

We assess freshwater pathway seasonal variations and spatial distributions in the NWGOA-HRB model integrations (Figure 11) by integrating the depth-dependent velocity and salinity field over the upper 50 m of the water column to form an estimate of the near-surface *FWT*:

$$FWT = \int_{-50}^{0} \frac{Sr - S}{Sr}[u + iv]dz \tag{1}$$

Here, $S = S(x, y, z, t)$ and $U = u + iv = U(x, y, z, t)$. Following Weingartner et al. (2005), we select a reference salinity of $S_r = 33.8$ that corresponds to the base of the permanent halocline in the GOA. *FWT* in the upper 50 m of the water column undergoes a pronounced annual cycle, with the largest transports occurring late in the year along the continental slope and over most of the shelf but during summer and fall in upper Cook Inlet.

Despite seasonal variability in coastal discharges and winds, the location of the mean modeled freshwater pathways varies only modestly from season to season. Stratification tends to decouple surface and near-bottom waters but FWT in the upper 50 m of the water column is still strongly controlled by the underlying bathymetry, as seen along the many canyons and adjoining banks that extend from Prince William Sound and Kodiak Island to the shelf break, along the continental slope, and down Shelikof Strait. Shoaled regions (e.g., Portlock and Albatross banks) tend to show a trapped anticyclonic FWT, while canyons show on-shelf freshwater flows along their eastern sidewalls and off-shelf flow along their western sidewalls. See Mordy et al. (2019) for additional discussion of the effects of bathymetric controls in the GOA.

Intraseasonal persistence in freshwater pathways dominates the structure but exceptions exist. We observe a change in flow direction along the Kodiak Island side of northern Shelikof Strait where the coastal flow field is directed to the SW for much of the year but to the NE in June (Figure 11b). We also note that the freshwater flow along the Kenai Peninsula in December is somewhat stronger and extends farther offshore than in the other months shown.

One location of particularly pronounced on-shelf freshwater flow occurs immediately east of Middleton Island, where satellite-tracked drifters commonly move from the slope flow onto the shelf (Royer et al., 1979; Stabeno et al., 2016) under the influence of topographic control, winds, or some other mechanism. This location may prove to be an important site of cross-shelf exchange, where waters may transition from the continental slope onto the shelf. Such a feature may provide a pathway to shelf and coastal habitats for oceanic-origin eggs, larvae, and plankton. Note the existence of two anticyclonic circulation cells on the NE shelf that emerge especially in the September climatology (Figure 11c): one between Kayak Island and the Copper River, and a second larger cell between Middleton Island and the coast. The southern portion of each of these cells reaches close to the shelf break and thus also represents potentially persistent pathways for the on-shelf advection of upper continental slope waters. Hydrography and thermal satellite images have shown Kayak Island in particular to be a recurring location of eddy formation (Ahlnäs et al., 1987; Royer et al., 1979).

4. Summary and Discussion

Relative to ocean circulation models forced with broadly distributed virtual precipitation, forcing an ocean circulation model with output from a land hydrography model by exchanging mass, momentum and tracers through the coastal sidewall provides a more realistic approach to modeling the distribution and fate of terrestrial snow melt, ice melt, and precipitation in the GOA. Our results suggest that this implementation will lead directly to better understandings of the regional circulation field and its roles in regulating the marine ecosystem. For example, the NWGOA-HRB implementation provides appreciably higher fidelity reproductions of the lateral and vertical salinity distribution fields. In turn, these distributions manifest as differences in the location and strength of sea surface elevation gradients, fronts, baroclinic jets, and the transport of planktonic and biogeochemical tracers. Modeling the exchange of limiting micronutrients into the high-chlorophyll-low-nutrient offshore waters of the central GOA depends critically upon the ability of a model to resolve mesoscale and submesoscale features and their associated density structure.

The virtual precipitation surface forcing approach is a common method of prescribing coastal runoff in GOA circulation models but it likely induces mismatch between the forcing and the associated hydrographic structure and flow dynamics and likely induces biogeochemical transformation mismatches across space and time in ecosystem modeling applications. In the real world, the distance offshore of the ACC density front varies seasonally, with it bottom-trapped and close to shore in winter but surface trapped and relaxed farther offshore in summer (Weingartner et al., 2002). Imposing fresh water at the surface based on a time-invariant cross-shelf decay scale results in seasonally differing fractions of the incoming fresh water being placed on either side of the front in a physically unrealistic fashion. Most importantly, the surface forcing approach does not allow ocean physics to fully control processes that induce cross-shelf dispersion and instead imposes dispersion characteristics that may not hold equally well under all wind and cross-shelf density gradient regimes nor in other domains with different mixing characteristics. The sidewall model forcing is thus superior for dynamical reasons, because it allows the runoff to disperse into the shelf structure as dictated by the governing physics.

The sidewall mass flux also allows one to specify parameter concentrations (e.g., heat, salinity, nutrients, and dissolved inorganic carbon) that can be directly measured in land runoff before it enters the ocean. For example, the inclusion of heat in river discharges has been shown to make a significance difference to ocean density, ice, and stratification fields relative to inflows without heat specified (Whitefield et al., 2015). In biogeochemical modeling applications the surface forcing approach precludes the ability for offshore-placed nutrients to undergo any time-dependent biogeochemical transformations in the nearshore zone. Consequently, the surface forcing limits our ability to accurately model ecosystem dynamics in the coastal zone. Hence, best practice for terrestrial-ocean coupling dictates that runoff (and its constituent

biogeochemical components) be incorporated at the right places so as to permit shelf fronts and stratification to develop according to physics.

Further improvements to the modeled circulation and hydrography will need to incorporate additional physical processes that the model presently lacks. As noted above, the NWGOA density field does not sufficiently destratify through fall months, thus driving a positive feedback that traps heat and fresh water near the surface and further increases stratification. We speculate that implementing surface mixing resulting from wind waves and swell could help address this problem, at the expense of additional computational resources. Also, if the actual coastal discharge is closer to that estimated with CFSR-driven forcing than the NARR forcing (Beamer et al., 2016), then the total discharge volume will modestly decrease and in turn benefit the modeled salinity and stratification fields.

Many aspects of these new model results require further investigation. Why does the nature of the discharge, with its strongest impact on the inner shelf, appear to have such a dramatic effect on the structure and velocity fields of a large mesoscale eddy (Figures 4i and 4j) located off the shelf (centered near 146°W, 58.5°N)? Why do some of the maximum correlations between observed and modeled temperatures occur at middepth levels? This result suggests that the model may well represent anomalies of interior lateral advection, even if the stratification is too strong on average. Finally, the importance of cross-shelf transport from the coastal zone via baroclinic eddy fluxes is still largely unknown but an eddy-resolving model configuration like the NWGOA-HRB coupling may address this and related biogeochemical cycling issues.

Our results suggest that the common approach to implementing coarse-resolution discharge estimates as surface salinity adjustments appears inadequate for many applications. Forcing ocean models through the sidewall with volume fluxes from the coarse global discharge models would circumvent issues specifically associated with virtual precipitation implementations, but an additional problem is that global models can be locally inaccurate due to lack of regional calibration and unrepresented sub-grid-scale processes. Global models tend to underestimate the total discharge from the GOA watershed and due to their spatial and temporal resolution they are unable to adequately pinpoint the location and timing of discharge events. Hence, it is the combination of using the sidewall mass flux boundary condition for coastal runoff along with well resolved runoff fields that generate the most realistic hindcast results. Ecosystem and ocean dynamics that depend on the timing, location, and strength of advective freshwater pathways may only be well resolved and understood through a coupled modeling approach that links high-resolution terrestrial hydrological and oceanic circulation models.

Data Availability Statement

All CTD data used in this manuscript are described in section 2.3, including internet addresses where these data can be obtained. Terrestrial discharge model data are available through AOOS (https://portal.aoos.org/#metadata/2c11c0f6-be73-4044-8dd2-55d8b59bb203). Ocean model code for the NEP and NWGOA models are available at Ocean model code, and helper files for the NEP and NWGOA models are available online (at 10.5281/zenodo.3661518 and 10.5281/zenodo.3708464). CTD data from Station GAK1 and along the Seward hydrographic line were collected with support from the Alaska Ocean Observing System, the North Pacific Research Board, the Exxon Valdez Oil Spill Trustee Council, and the National Science Foundation.

References

Ahlnäs, K., Royer, T. C., & George, T. H. (1987). Multiple dipole eddies in the Alaska Coastal Current detected with Landsat thematic mapper data. *Journal of Geophysical Research*, *92*(C12), 13,041–13,047. https://doi.org/10.1029/JC092iC12p13041

Arendt, A., Luthcke, S., Gardner, A., O'Neel, S., Hill, D., Moholdt, G., et al. (2013). Analysis of a GRACE global mascon solution for Gulf of Alaska glaciers. *Journal of Glaciology*, *59*, 913–924. https://doi.org/10.3189/2013JoG12J197

Beamer, J., Hill, D. F., Arendt, A., & Liston, G. (2016). High-resolution modeling of coastal freshwater discharge and glacier mass balance in the Gulf of Alaska watershed. *Water Resources Research*, *52*, 3888–3909. https://doi.org/10.1002/2015WR018457

Boyer, T. P., Antonov, J. I., Baranova, O. K., Coleman, C., Garcia, H. E., Grodsky, A., et al. (2013). *World Ocean Database 2013, NOAA Atlas NESDIS 72* (Technical ed., pp. 1–209). Silver Spring, MD. https://doi.org/10.7289/V5NZ85MT

Carmack, E. C. (2007). The alpha/beta ocean distinction: A perspective on freshwater fluxes, convection, nutrients, and productivity in high-latitude seas. *Deep-Sea Research Part II*, *54*(23-26), 2578–2598. https://doi.org/10.1016/j.dsr2.2007.08.018

Carton, J. A., Chepurin, G., Cao, X., & Giese, B. S. (2000). A Simple Ocean Data Assimilation analysis of the global upper ocean 1950–1995, Part 1: Methodology. *Journal of Physical Oceanography*, *30*(2), 294–309. https://doi.org/10.1175/1520-0485(2000)030<0294:ASODAA>2.0.CO;2

Colas, F., Wang, X., Capet, X., Chao, Y., & McWilliams, J. C. (2013). Untangling the roles of wind, run-off and tides in Prince William sound. *Continental Shelf Research*, *63*, S79–S89, ISSN 0278-4343. https://doi.org/10.1016/j.csr.2012.05.002

Coyle, K. O., Cheng, W., Hinckley, S., Lessard, E. J., Whitledge, T., Hermann, A. J., & Hedstrom, K. (2012). Model and field observations of effects of circulation on the timing and magnitude of nitrate utilization and production on the northern Gulf of Alaska shelf. *Progress in Oceanography*, *103*, 16–41. https://doi.org/10.1016/j.pocean.2012.03.002

Coyle, K. O., Hermann, A. J., & Hopcroft, R. R. (2019). Modeled spatial-temporal distribution of productivity, chlorophyll, iron and nitrate on the northern Gulf of Alaska shelf relative to field observations. *Deep Sea Research Part II: Topical Studies in Oceanography*, *165*, 163–191. https://doi.org/10.1016/j.dsr2.2019.05.006

Curchitser, E. N., Haidvogel, D. B., Hermann, A. J., Dobbins, E. L., Powell, T. M., & Kaplan, A. (2005). Multi-scale modeling of the North Pacific Ocean: Assessment and analysis of simulated basin-scale variability (1996–2003). *Journal of Geophysical Research*, *110*, C11021. https://doi.org/10.1029/2005JC002902

Dai, A., Qian, T., Trenberth, K. E., & Milliman, J. D. (2009). Changes in continental freshwater discharge from 1948–2004. *Journal of Climate*, *22*(10), 2773–2792. https://doi.org/10.1175/2008JCLI2592.1

Dai, A., & Trenberth, K. E. (2002). Estimates of freshwater discharge from continents: Latitudinal and seasonal variations. *Journal of Hydrometeorology*, *3*(6), 660–687. https://doi.org/10.1175/1525-7541(2002)003<0660:EOFDFC>2.0.CO;2

Daly, C., Neilson, R. P., & Phillips, D. L. (1994). A statistical-topographic model for mapping climatological precipitation over mountainous terrain. *Journal of Applied Meteorology*, *33*(2), 140–158. https://doi.org/10.1175/1520-0450

Danielson, S., Curchitser, E., Hedstrom, K., Weingartner, T., & Stabeno, P. (2011). On ocean and sea ice modes of variability in the Bering Sea. *Journal of Geophysical Research*, *116*, C12034. https://doi.org/10.1029/2011jc007389

Danielson, S., Hedstrom, K., Aagaard, K., Weingartner, T., & Curchitser, E. (2012). Wind-induced reorganization of the Bering shelf circulation. *Geophysical Research Letters*, *39*, L08601. https://doi.org/10.1029/2012GL051231

Dissing, D., & Wendler, G. (1998). Solar radiation climatology of Alaska. *Theoretical and Applied Climatology*, *61*(3-4), 161–175. https://doi.org/10.1007/s007040050061

Dobbins, E. L., Hermann, A. J., Stabeno, P. J., Bond, N. A., & Steed, R. C. (2009). Modeled transport of freshwater from a line-source in the coastal Gulf of Alaska. *Deep Sea Research, Part II*, *56*(24), 2409–2426. https://doi.org/10.1016/j.dsr2.2009.02.004

Egbert, G. D., & Erofeeva, S. Y. (2002). Efficient inverse modeling of barotropic ocean tides. *Journal of Atmospheric and Oceanic Technology*, *19*, 183–204. https://doi.org/10.1175/1520-0426(2002)019<0183:EIMOBO>2.0.CO;2

Ek, M. B., Mitchell, K. E., Lin, Y., Rogers, E., Grunmann, P., Koren, V., et al. (2003). Implementation of Noah land surface model advances in the National Centers for Environmental Prediction operational mesoscale Eta model. *Journal of Geophysical Research*, *108*(D22), 8851. https://doi.org/10.1029/2002JD003296

Farrara, J. D., Chao, Y., Li, Z., Wang, X., Jin, X., Zhang, H., et al. (2013). A data-assimilative ocean forecasting system for the Prince William Sound and an evaluation of its performance during Sound Predictions 2009. *Continental Shelf Research*, *63*(2013), S193–S208. https://doi.org/10.1016/j.csr.2012.11.008

Fekete, B. M., Vörösmarty, C. J., & Grabs, W. (2002). High-resolution fields of global runoff combining observed river discharge and simulated water balances. *Global Biogeochemical Cycles*, *16*(3), 15–11. https://doi.org/10.1029/1999GB001254

Fissel, B., Dalton, M., Garber-Yonts, B., Haynie, A., Kasperski, S., Lee, J., et al. (2017). Stock assessment and fishery evaluation report for the groundfish fisheries of the Gulf of Alaska and Bering Sea/Aleutian Island area: Economic status of the groundfish fisheries off Alaska, 2016 (pp. 1–425). Seattle, WA: Alaska Fisheries Science Center, National Marine Fisheries Service National Oceanic and Atmospheric Administration.

Foreman, M. G. G., Crawford, W. R., Cherniawsky, J. Y., Henry, R. F., & Tarbotton, M. R. (2000). A high-resolution assimilating tidal model for the northeast Pacific Ocean. *Journal of Geophysical Research: Oceans*, *105*(C12), 28,629–28,651. https://doi.org/10.1029/1999jc000122

Freeland, H., Denman, K., Wong, C. S., Whitney, F., & Jacques, R. (1997). Evidence of change in the winter mixed layer in the Northeast Pacific Ocean. *Deep Sea Research Part I: Oceanographic Research Papers*, *44*(12), 2117–2129. https://doi.org/10.1016/S0967-0637(97)00083-6

Galt, J. A. W., Lehr, J., & Payton, D. L. (1991). Fate and transport of the Exxon Valdez oil spill. *Environmental Science and Technology*, *25*(2), 202–209. https://doi.org/10.1021/es00014a001

Halverson, M. J., Bélanger, C., & Gay, S. M. (2013). Seasonal transport variations in the straits connecting Prince William Sound to the Gulf of Alaska. *Continental Shelf Research*, *63*, S63–S78. https://doi.org/10.1016/j.csr.2012.06.017

Hedström, K. (2018). *Technical manual for a coupled sea-ice/ocean circulation model (Version 5)* (pp. 1–176). Anchorage, Alaska: U.S. Department of the Interior, Bureau of Ocean Energy Management.

Henson, S. A. (2007). Water column stability and spring bloom dynamics in the Gulf of Alaska. *Journal of Marine Research*, *65*(6), 715–736. https://doi.org/10.1357/002224007784219002

Hermann, A. J., Hinckley, S., Dobbins, E. L., Haidvogel, D. B., Bond, N. A., Mordy, C., et al. (2009). Quantifying cross-shelf and vertical nutrient flux in the coastal Gulf of Alaska with a spatially nested, coupled biophysical model. *Deep Sea Research Part II: Topical Studies in Oceanography*, *56*(24), 2474–2486. https://doi.org/10.1016/j.dsr2.2009.02.008

Hermann, A. J., Ladd, C., Cheng, W., Curchitser, E. N., & Hedstrom, K. (2016). A model-based examination of multivariate physical modes in the Gulf of Alaska. *Deep Sea Research Part II: Topical Studies in Oceanography*, *132*, 68–89. https://doi.org/10.1016/j.dsr2.2016.04.005

Hill, D. F., Bruhis, N., Calos, S. E., Arendt, A., & Beamer, J. (2015). Spatial and temporal variability of freshwater discharge into the Gulf of Alaska. *Journal of Geophysical Research: Oceans*, *120*, 634–646. https://doi.org/10.1002/2014JC010395

Jacob, T., Wahr, J., Pfeffer, W. T., & Swenson, S. (2012). Recent contributions of glaciers and ice caps to sea level rise. *Nature*, *482*(7386), 514.

Janout, M. A., Weingartner, T. J., Royer, T. C., & Danielson, S. L. (2010). On the nature of winter cooling and the recent temperature shift on the northern Gulf of Alaska shelf. *Journal of Geophysical Research*, *115*, C05023. https://doi.org/10.1029/2009jc005774

Johnson, W. R., Royer, T. C., & Luick, J. L. (1988). On the seasonal variability of the Alaska Coastal Current. *Journal of Geophysical Research*, *93*(C10), 12,423–12,437. https://doi.org/10.1029/jc093ic10p12423

Kelley, J. (2015). *An examination of hydrography and sea level in the Gulf of Alaska (M.S. thesis)*. Fairbanks, Alaska: University of Alaska Fairbanks. https://hdl.handle.net/11122/5746

Ladd, C., Stabeno, P., & Cokelet, E. D. (2005). A note on cross-shelf exchange in the northern Gulf of Alaska. *Deep Sea Research Part II: Topical Studies in Oceanography*, *52*(5-6), 667–679. https://doi.org/10.1016/j.dsr2.2004.12.022

Large, W. G., & Yeager, S. G. (2009). The global climatology of an interannually varying air-sea flux data set. *Climate Dynamics*, *33*(2-3), 341–364. https://doi.org/10.1007/s00382-008-0441-3

Larsen, C. F., Burgess, E., Arendt, A. A., O'Neel, S., Johnson, A. J., & Kienholz, C. (2015). Surface melt dominates Alaska glacier mass balance. *Geophysical Research Letters*, *42*, 5902–5908. https://doi.org/10.1002/2015GL064349

Liston, G. E., & Elder, K. (2006a). A meteorological distribution system for high-resolution terrestrial modeling (MicroMet). *Journal of Hydrometeorology*, *7*(2), 217–234. https://doi.org/10.1175/JHM486.1

Liston, G. E., & Elder, K. (2006b). A distributed snow-evolution modeling system (SnowModel). *Journal of Hydrometeorology*, *7*(6), 1259–1276. https://doi.org/10.1175/JHM548.1

Liston, G. E., & Mernild, S. H. (2012). Greenland freshwater runoff. Part I: A runoff routing model for glaciated and nonglaciated landscapes (HydroFlow). *Journal of Climate*, *25*(17), 5997–6014. https://doi.org/10.1175/JCLI-D-11-00591.1

Marchesiello, P., McWilliams, J. C., & Shchepetkin, A. F. (2001). Open boundary conditions for long-term integration of regional ocean models. *Ocean Modelling*, *3*(1-2), 1–20. https://doi.org/10.1016/S1463-5003(00)00013-5

Mesinger, F., DiMego, G., Kalnay, E., Mitchell, K., Shafran, P. C., Ebisuzaki, W., et al. (2006). North American Regional Reanalysis. *Bulletin of the American Meteorological Society*, *87*(3), 343–360. https://doi.org/10.1175/BAMS-87-3-343

Mordy, C. W., Stabeno, P. J., Kachel, N. B., Kachel, D., Ladd, C., Zimmermann, M., et al. (2019). Patterns of flow in the canyons of the northern Gulf of Alaska. *Deep Sea Research Part II: Topical Studies in Oceanography*, *165*, 203–220. https://doi.org/10.1016/j.dsr2.2019.03.009

Muench, R. D., & Schumacher, J. D. (1980). *Physical oceanographic and meteorological conditions in the northwest Gulf of Alaska (Tech. Memo. ERL PMEL-22)* (pp. 1–147). Silver Spring, MD: National Oceanic and Atmospheric Administration.

Neal, E. G., Hood, E., & Smikrud, K. (2010). Contribution of glacier runoff to freshwater discharge into the Gulf of Alaska. *Geophysical Research Letters*, *37*, L06404. https://doi.org/10.1029/2010GL042385

Niebauer, H. J., Royer, T. C., & Weingartner, T. J. (1994). Circulation of Prince William Sound, Alaska. *Journal of Geophysical Research*, *99*(C7), 14,113–14,126. https://doi.org/10.1029/94jc00712

Okkonen, S. R., Pegau, S., & Saupe, S. (2009). *Seasonality of boundary conditions for Cook Inlet, Alaska* (pp. 1–64). Fairbanks, Alaska: University of Alaska Fairbanks.

Pawlowicz, R., Beardsley, B., & Lentz, S. (2002). Classical tidal harmonic analysis including error estimates in MATLAB using T_TIDE. *Computers & Geosciences*, *28*(8), 929–937. https://doi.org/10.1016/S0098-3004(02)00013-4

Reed, R. K. (1984). Flow of the Alaskan Stream and its variations. *Deep Sea Research Part A. Oceanographic Research Papers*, *31*(4), 369–386. https://doi.org/10.1016/0198-0149(84)90090-6

Rienecker, M. M., Suarez, M. J., Gelaro, R., Todling, R., Bacmeister, J., Liu, E., et al. (2011). MERRA: NASA's Modern-Era Retrospective Analysis for Research and Applications. *Journal of Climate*, *24*(14), 3624–3648. https://doi.org/10.1175/JCLI-D-11-00015.1

Royer, T. C. (1979). On the effect of precipitation and runoff on coastal circulation in the Gulf of Alaska. *Journal of Physical Oceanography*, *9*(3), 555–563. https://doi.org/10.1175/1520-0485(1979)009<0555:OTEOPA>2.0.CO;2

Royer, T. C. (1982). Coastal fresh water discharge in the northeast Pacific. *Journal of Geophysical Research*, *87*(C3), 2017–2021. https://doi.org/10.1029/JC087iC03p02017

Royer, T. C., & Grosch, C. E. (2006). Ocean warming and freshening in the northern Gulf of Alaska. *Geophysical Research Letters*, *33*, L16605. https://doi.org/10.1029/2006GL026767

Royer, T. C., Hansen, D. V., & Pashinski, D. J. (1979). Coastal flow in the northern Gulf of Alaska as observed by dynamic topography and satellite-tracked drogued drift buoys. *Journal of Physical Oceanography*, *9*(4), 785–801. https://doi.org/10.1175/1520-0485(1979)009<0785:CFITNG>2.0.CO;2

Saha, S., Moorthi, S., Pan, H. L., Wu, X., Wang, J., Nadiga, S., et al. (2010). The NCEP climate forecast system reanalysis. *Bulletin of the American Meteorological Society*, *91*(8), 1015–1058. https://doi.org/10.1175/2010BAMS3001.1

Shchepetkin, A. F., & McWilliams, J. C. (2005). The Regional Ocean Modeling System: A split-explicit, free-surface, topography-following-coordinate ocean model. *Ocean Model*, *9*(4), 347–404. https://doi.org/10.1016/j.ocemod.2004.08.002

Siedlecki, S. A., Pilcher, D. J., Hermann, A. J., Coyle, K., & Mathis, J. (2017). The importance of freshwater to spatial variability of aragonite saturation state in the Gulf of Alaska. *Journal of Geophysical Research: Oceans*, *122*, 8482–8502. https://doi.org/10.1002/2017JC012791

Simpson, J. H. (1997). Physical processes in the ROFI regime. *Journal of Marine Systems*, *12*(1–4), 3–15. https://doi.org/10.1016/S0924-7963(96)00085-1

Simpson, J. H., Sharples, J., & Rippeth, T. (1991). A prescriptive model of stratification induced by freshwater runoff. *Estuarine, Coastal and Shelf Science*, *33*(1), 23–35. https://doi.org/10.1016/0272-7714(91)90068-M

Smith, W. H. F., & Sandwell, D. T. (1997). Global sea floor topography from satellite altimetry and ship depth soundings. *Science*, *277*(5334), 1956–1962. https://doi.org/10.1126/science.277.5334.1956

Spall, M. A., & Chapman, D. C. (1998). On the efficiency of baroclinic eddy heat transport across narrow fronts. *Journal of Physical Oceanography*, *28*(11), 2275–2287. https://doi.org/10.1175/1520-0485(1998)028<2275:oteobe>2.0.co;2

Stabeno, P. J., Bell, S., Cheng, W., Danielson, S., Kachel, N. B., & Mordy, C. W. (2016). Long-term observations of Alaska Coastal Current in the northern Gulf of Alaska. *Deep-Sea Research Part II*, *132*(2016-a), 24–40. https://doi.org/10.1016/j.dsr2.2015.12.016

Strom, S. L., Fredrickson, K. A., & Bright, K. J. (2016). Spring phytoplankton in the eastern coastal Gulf of Alaska: Photosynthesis and production during high and low bloom years. *Deep Sea Research Part II: Topical Studies in Oceanography*, *132*, 107–121. https://doi.org/10.1016/j.dsr2.2015.05.003

Umlauf, L., & Burchard, H. (2003). A generic length-scale equation for geophysical turbulence models. *Journal of Marine Research*, *61*(2), 235–265. https://doi.org/10.1357/002224003322005087

Wang, J., Jin, M., Musgrave, D., & Ikeda, M. (2004). A hydrological digital elevation model for freshwater discharge into the Gulf of Alaska. *Journal of Geophysical Research*, *109*, C07009. https://doi.org/10.1029/2002JC001430

Wang, Y., Xue, H., Chai, F., Chao, Y., & Farrara, J. (2014). A model study of the Copper River plume and its effects on the northern Gulf of Alaska. *Ocean Dynamics*, *64*(2), 241–258. https://doi.org/10.1007/s10236-013-0684-3

Warner, J. C., Defne, Z., Haas, K., & Arango, H. G. (2013). A wetting and drying scheme for ROMS. *Computers & Geosciences*, *58*, 54–61, ISSN 0098–3004. https://doi.org/10.1016/j.cageo.2013.05.004

Warner, J. C., Sherwood, C. R., Arango, H. G., & Signell, R. P. (2005). Performance of four turbulence closure models implemented using a generic length scale method. *Ocean Modelling*, *8*(1-2), 81–113. https://doi.org/10.1016/j.ocemod.2003.12.003

Weingartner, T. J., Coyle, K., Finney, B., Hopcroft, R., Whitledge, T., Brodeur, R., et al. (2002). The Northeast Pacific GLOBEC Program: Coastal Gulf of Alaska. *Oceanography*, *15*(2), 48–63. https://doi.org/10.5670/oceanog.2002.21

Weingartner, T. J., Danielson, S. L., & Royer, T. C. (2005). Freshwater variability and predictability in the Alaska Coastal Current. *Deep Sea Research, Part II*, *52*(1-2), 169–191. https://doi.org/10.1016/j.dsr2.2004.09.030

Whitefield, J., Winsor, P., McClelland, J. W., & Menemenlis, D. (2015). A new river discharge and river temperature climatology data set for the pan-arctic region. *Ocean Modelling*, *88*, 1–15. https://doi.org/10.1016/j.ocemod.2014.12.012

Williams, W. J., Weingartner, T. J., & Hermann, A. J. (2007). Idealized three-dimensional modeling of seasonal variation in the Alaska Coastal Current. *Journal of Geophysical Research*, *112*, C07001. https://doi.org/10.1029/2005JC003285

Wilson, J. G., & Overland, J. E. (1986). Meteorology. In D. W. Hood, & S. T. Zimmerman (Eds.), *The Gulf of Alaska, physical environment and biological resources* (pp. 31–53). Springfield, VA: Alaska Office, Ocean Assessments Division, National Oceanic and Atmospheric Administration, US Department of Commerce.